Nanoscale

Accepted Manuscript

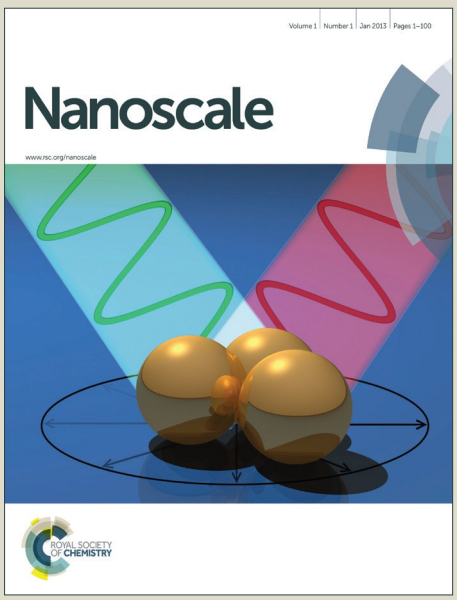

ROYAL SOCIETY OF CHEMISTRY

www.rsc.org/nanoscale

Journal Name

ARTICLE

Highly Branched PtCu Bimetallic Alloy Nanodendrites with Superior Electrocatalytic Activities for Oxygen Reduction Reaction

Received 00th January 20xx,
Accepted 00th January 20xx

DOI: 10.1039/x0xx00000x

www.rsc.org/

Shaofang Fu,[a] Chengzhou Zhu,[*a] Qiurong Shi,[a] Haibing Xia,[c] Dan Du,[a] Yuehe Lin[*a,b]

Morphology controlling is a promising strategy to improve the catalytic performance of Pt-based catalysts. In this work, we reported a facile synthesis of PtCu bimetallic alloy nanodendrites using Brij 58 as template. The highly branched structures and porous features offer relatively large surface areas, which is beneficial to the enhancement of catalytic activity for oxygen reduction reaction in fuel cells. In addition, the elimination of carbon supports showed an important effect on the stability of the catalysts. By tuning the ratio of Pt and Cu precursors, PtCu nanodendrites were almost four times more active on the basis of equivalent Pt mass for oxygen reduction reaction than the commercial Pt/C catalyst.

Introduction

Proton exchange membrane fuel cells (PEMFCs) are considered as potential power sources for automobiles and portable electronic devices.[1, 2] To date, Pt-based materials are the most effective catalysts for both hydrogen oxidation and oxygen reduction reaction (ORR).[3, 4] However, the commercialization of PEMFCs is still hindered by some critical issues, including the high cost of Pt and the sluggish ORR kinetics. [5, 6] Control of nanostructures at the atomic level for optimizing the structural and compositional effect and therefore precisely and effectively tuning catalytic properties of Pt-based catalysts have been achieved through the synthesis of functional Pt nanoparticles, bimetallic/multimetallic Pt alloys, core–shell structures, and novel supporting nanomaterials.[4, 7] Among them, alloying Pt with nonprecious transition metals (Co, Cu, Ni, Cu, etc.) to form bimetallic/multimetallic alloys is considered to be one of the most effective strategies to improve the electrocatalytic properties of Pt-based materials.[8-11] This approach could not only reduce the cost by substituting partial Pt with nonprecious metals, but also improve the electrocatalytic ORR performance of Pt-based catalysts compared to monometallic Pt nanomaterials. It is believed that the enhanced catalytic properties of alloy nanostructures are closely associated with the geometric effect, which is caused by the change in electronic structure resulting from surface compression/expansion.[12, 13] Like other catalytic systems, ORR is one of the most structure-sensitive reactions, which makes the rational design of Pt-based nanostructures with a controlled shape and size a versatile knob for tuning their electrocatalytic performance.[14] The typical example is that Chen et al. synthesized Pt_3Ni nanoframes by interior erosion of crystalline $PtNi_3$ polyhedra.[4] Both the interior and exterior surfaces of this nanoframe are composed of the nanosegregated Pt-skin structure, which achieved a factor of 36 enhancement in mass activity and a factor of 22 enhancement in specific activity, respectively for ORR. In another report, Huang et al. also presented an efficient strategy for the preparation of Pt_3Ni nanocrystals with highly porous feature, which were served as highly efficient catalysts in ORR with much better performance than commercial Pt/C catalysts.[5] In general, Pt-based nanomaterials with dendritic structures, synthesized using either template or template-free route,[5, 15-17] have attracted extensive attentions on electrocatalysts. The porous nanodendrites (NDs) with interconnected branches provide a novel strategy to improve the surface area of Pt-based nanomaterials. Moreover, the open structures are also favorable for the interaction between Pt catalyst and guest species.[18]

Herein, PtCu bimetallic alloy nanodendrites (BANDs) were synthesized by an efficient one-step route, where Pt and Cu precursors were reduced within 30 min using Brij 58 as the template. Porous PtCu BANDs with high surface area in high yield (~ 100%) were obtained by rational tuning the ratio between Pt and Cu precursors. Furthermore, the as-prepared PtCu BANDs exhibited superior electrocatalytic activity and durability toward ORR compared to commercial Pt/C catalyst. The proposed approach not only provides a novel method to synthesize PtCu BANDs, but also offers a promising design of nanomaterials with controllable compositions and structures.

Experimental Section

[a] The School of Mechanical and Materials Engineering, Washington State University, Pullman, Washington 99164, United States.
[b] Pacific Northwest National Laboratory, Richland, Washington 99352, United States.
[c] State Key Laboratory of Crystal Materials, Shandong University, Jinan, P. R. China.
Electronic Supplementary Information (ESI) available: [details of any supplementary information available should be included here]. See DOI: 10.1039/x0xx00000x

Chemicals and Reagents

Commercial platinum/carbon (Pt/C) (Pt loading: 20 wt. %, Pt on carbon black) was purchased from Alfa Aesar. Copper (II) chloride ($CuCl_2$, powder, 99%), potassium tetrachloroplatinate (II) (K_2PtCl_4, 98%), potassium chloride (KCl, 99.0~100.5%), nafion perfluorinated resin solution (5 wt. % in mixture of lower aliphatic alcohols and water, contains 45% water), Brij 58 (average M_n ~1124) and perchloric acid ($HClO_4$) were obtained from Sigma-Aldrich. L(+)-ascorbic acid (AA, $C_6H_8O_6$) was from Acros organics. All aqueous solutions were prepared with ultrapure water (>18 MΩ) from a Milli-Q system.

Characterization

Transmission electron microscopy (TEM) images were obtained by Philips CM200 UT (Field Emission Instruments, USA). High-resolution TEM (HRTEM) images were obtained with a JEOL JEM 2100F TEM at an accelerating voltage of 200 kV. High-angle annular dark-field scanning transmission electron microscopy (HAADF-STEM) and elemental mapping images were acquired by energy dispersive X-ray spectroscopy (EDS) using a JEOL-2100F electron microscope equipped with a STEM unit. FEI Sirion field emission scanning electron microscope (FESEM) was used for energy-dispersive X-ray analysis (EDX). X-ray Diffraction (XRD) characterization was carried out by Rigaku Miniflex 600. The tube was operated at 40 kV accelerating voltage and 15 mA current. X-ray photoelectron spectroscopy (XPS) measurements were performed on a Kratos AXIS-165 multi-technique electron spectrometer system with a base pressure of $1x10^{-9}$ torr. The spectra of the surfaces were obtained with an AXIS-165 manufactured by Kratos Analytical Inc. (Spring Valley, NY, USA) using a monochromatic X-ray radiation of 1487 eV (Al Kα). The spectrometer was calibrated against both the Au $4f_{7/2}$ peak at 84.0 eV and the Ag $3d_{5/2}$ peak at 368.3 eV. Static charging when present was corrected with a neutralizer (flood gun) by placing the carbon peak (C 1s) at about 285 eV.

Synthesis of Pt NDs and PtCu BANDs

To synthesize typical PtCu BANDs, 2.5 mL of aqueous solution containing 15 mM K_2PtCl_4, 5 mM $CuCl_2$ and 5 mg/mL Brij 58 was placed in a vial and heated to 60 °C with stirring using a water bath. Then, 2.5 mL of 0.1 M AA was added into the previous solution quickly. After 30 min, the product was centrifuged at 10000 rpm for 10 min, followed by washing/centrifugation cycles to remove all residual impurities. The final product was dispersed into water for further use. In addition, pure Pt NDs and other PtCu BANDs were synthesized by setting the ratios between Pt and Cu precursors to be 1:0, 1:1 and 1:3 using the same procedure.

Electrocatalytic experiments

A glassy carbon rotating disk electrode (RDE, 5 mm in diameter) was polished and cleaned before surface coating. The PtCu BANDs (10 µL, 0.5 mg/mL with respect to Pt) were coated on the surface of pretreated RDE surface and dried at room temperature. After that, the modified RDE was covered with a layer of nafion (5 µL, 0.05%), followed by drying at room temperature. For commercial Pt/C catalyst (2 mg/mL), Pt/C powder was first dissolved into nafion solution containing nafion, 2-proponal, and water (v/v/v = 0.025/1/4). 10 µL of Pt/C catalyst was then dropped on the surface of pretreated RDE surface and dried before the electrocatalytic tests.

The electrochemical measurements were carried out by an electrochemical workstation (CHI 630E) coupled with a three-electrode system. Ag/AgCl electrode filled with saturated KCl aqueous solution and Pt wire were used as reference electrode and counter electrode, respectively.

Results and discussions

A variety of works have been reported on the synthesis of highly branched noble metal nanocrystals as well as noble metal based alloys, which have been applied on catalytic area.[17] However, these materials are synthesized either in organic solution or at high temperature.[18-21] There are still rare works focusing on the simple synthesis of high branched nanocrystal alloys involving Pt/nonprecious metal in aqueous solution with low temperature. In this work, PtCu BANDs were obtained by a simple chemical reduction method in aqueous solution, which was mediated by Brij 58. The composition of PtCu BANDs could be easily altered by changing the ratio of precursors. When the ratios were tuned to be 3:1, 1:1 and 1:3, $Pt_{78}Cu_{22}$, $Pt_{54}Cu_{46}$ and $Pt_{37}Cu_{63}$ BANDs were obtained by EDX analysis. The characteristic spectrum of $Pt_{78}Cu_{22}$ BANDs was shown in Figure S1. It should be noted that the as-prepared PtCu BANDs have a higher Pt composition in the whole range of precursor compositions ($PtCl_4^{2-}/Cu^{2+}$=3:1 to 1:3). Considering the standard reduction potential of $PtCl_4^{2-}$/Pt (+0.73 V vs. standard hydrogen electrode (SHE)) is higher than that of Cu^{2+}/Cu (+0.337 V vs. SHE), Pt reduction is much more preferred to that of Cu.

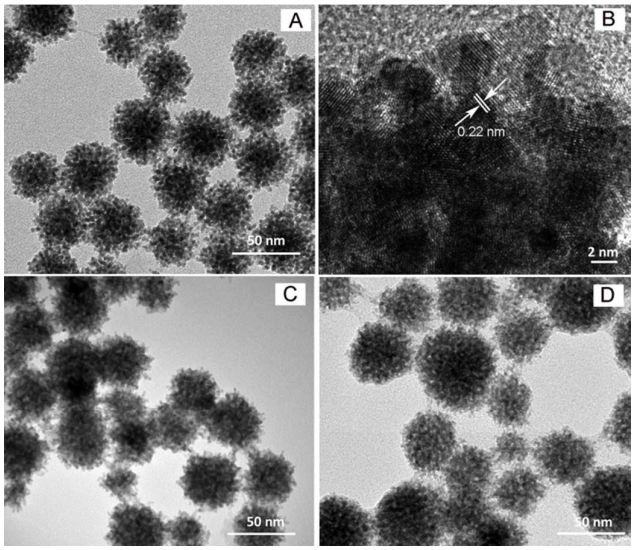

Figure 1. TEM images of $Pt_{78}Cu_{22}$ (A), $Pt_{54}Cu_{46}$ (C) and $Pt_{37}Cu_{63}$ (D) BANDs. (B) HRTEM of $Pt_{78}Cu_{22}$ BANDs.

The TEM images of Pt NDs and PtCu BANDs are shown in Figure 1 and S2. It reveals that the as-prepared $Pt_{78}Cu_{22}$ BANDs

are composed of uniform NDs with a yield around 100% which are highly monodispersed with an average size of 35 nm. The HRTEM image presents that the interplanar spacing is ~0.22 nm, corresponding to (111) crystal plane of PtCu alloys. According to the seeding/autocatalytic growth mechanism,[5, 22] Pt nanoparticle seeds with a low concentration were formed in the first step, where Pt precursors were reduced by AA. The formed Pt seeds will then become the catalysts for the co-reduction of $PtCl_4^{2-}$ and Cu^{2+}. Interestingly, the dendritic $Pt_{54}Cu_{46}$ and $Pt_{37}Cu_{63}$ BANDs could also be obtained by simply altering the molar ratios of metal precursors. However, the dendritic structures of $Pt_{54}Cu_{46}$ and $Pt_{37}Cu_{63}$ BANDs were not as uniform as that of $Pt_{78}Cu_{22}$ BANDs. Increasing the content of Cu precursors was not favorable for the dendrite nature, indicating that Pt precursor has a critical impact on the growth of PtCu BANDs. In this system, the concentration used was much higher than the critical micelle concentration (CMC). It is supposed that BANDs were formed by assembly of Brij 58 micelles with metal species. In the solution, the metallic ions, which are coordinated by water molecules to form metal-aqua complexes, adsorb inside the external ethylene oxide (EO) region of the micelles because the coordinated water molecules usually interact with EO groups. Therefore, it is reasonable to speculate that Brij 58 micelles served as the structural direct agent in the synthesis process.[23] The elemental mapping images in Figure 2 reveal that Pt and Cu are uniformly distributed through the entire dendritic structure, implying the formation of PtCu alloys.

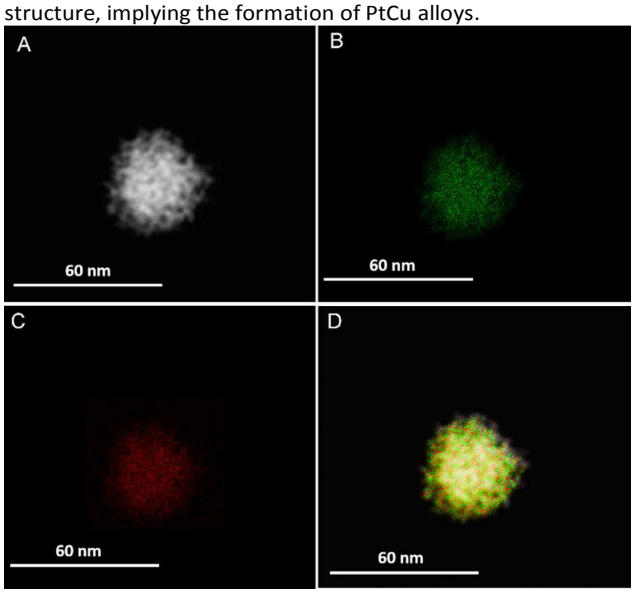

Figure 2. (A) HAADF-STEM and EDS elemental mapping images of Pt (B), Cu (C), and overlap (D) in $Pt_{78}Cu_{22}$ BANDs.

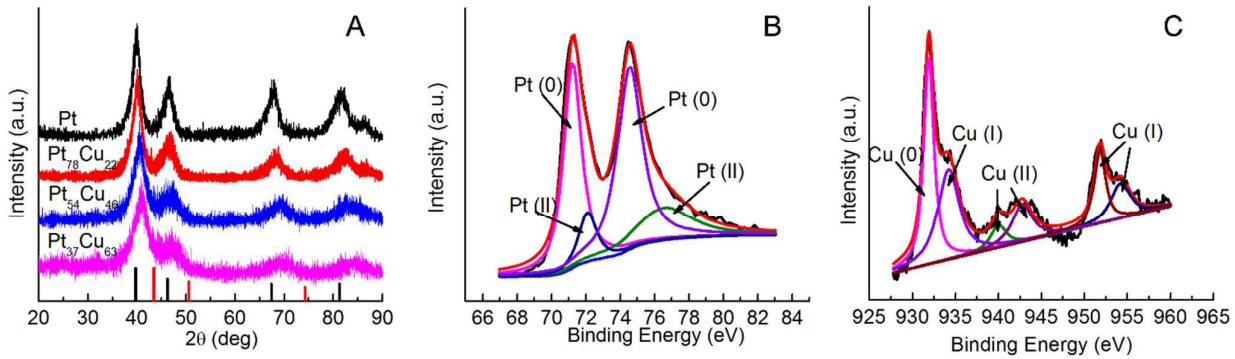

Figure 3. (A) XRD patterns of Pt NDs, $Pt_{78}Cu_{22}$, $Pt_{54}Cu_{46}$ and $Pt_{37}Cu_{63}$ BANDs (black: Pt, PDF #04-0802, red: Cu, PDF #65-9026). XPS spectra of Pt (B) and Cu (C) in $Pt_{78}Cu_{22}$ BANDs.

The crystalline structures of PtCu BANDs with different composition were analyzed by XRD. The patterns of PtCu BANDs present distinct peaks as shown in Figure 3A. The XRD pattern of $Pt_{78}Cu_{22}$ BANDs shows a typical fcc structure with peaks located at 2θ = 40.17, 46.58, 68.17, and 82.25°, corresponding to (111), (200), (220), and (311) planes, which are between those of pure Pt (black) and Cu (red). On the other hand, there is no Cu peak observed in the pattern demonstrating incorporation of Cu into the Pt lattice to form PtCu alloys in the $Pt_{78}Cu_{22}$ BANDs. Compared to $Pt_{78}Cu_{22}$ BANDs, the peak locations of $Pt_{54}Cu_{46}$ and $Pt_{37}Cu_{63}$ BANDs shift to higher diffraction angle due to the higher content of Cu.

To investigate the element compositions on the surface of PtCu BANDs, XPS analysis were carried out for the further characterization. For all the BANDs samples, the XPS spectra reveal the presence of Pt and Cu, as shown in Figure S3. The two peaks at 71.3 and 74.5 eV for $Pt_{78}Cu_{22}$ BANDs in Figure 3B correspond to Pt $4f_{7/2}$ and Pt $4f_{5/2}$, which could be further divided into four peaks at 71.2, 72.1, 74.6, and 76.6 eV, indicating the existence of metallic Pt and $PtO/Pt(OH)_2$.[24] According to the peak areas, Pt (0) is the dominant state in $Pt_{78}Cu_{22}$ BANDs, which is favorable for ORR. Figure 3C shows the high resolution XPS spectrum of Cu in $Pt_{78}Cu_{22}$ BANDs. The peaks at ~932 and ~952 eV in Figure 3C correspond to Cu $2p_{3/2}$ and Cu $2p_{1/2}$. It reveals the existence of metallic Cu as well as oxidized states, Cu (I) and Cu (II), which indicates the presence of Cu oxides and hydroxides on the surface of the BANDs.[25-27] By virtue of their large surface area and highly open structures, the PtCu BANDs are expected to have high surface area, and thus exhibit good electrocatalytic performance. The catalytic activities were measured and compared with commercial Pt/C catalyst. Cyclic voltammetry (CV) curves from 0.1~1.3 V vs. reversible hydrogen electrode (RHE) were obtained in N_2-saturated 0.1 M $HClO_4$ solution, as shown in Figure 4A. The

features of CV curves are similar for each catalyst: the hydrogen adsorption/desorption was observed in the potential range from 0.1 to 0.5 V. From 0.5 to 0.8 V is the double-layer capacitance region. Pt oxides were formed above 0.8 V. In the cathodic scan, the reduction of Pt oxides occurred. By quantifying the electric charges associated with hydrogen adsorption/desorption process, the electrochemical surface area (ECSA) could be obtained by assuming a value of 210 $\mu C/cm^2$ for the adsorption of a hydrogen monolayer. The calculated ECSA for Pt NDs, $Pt_{78}Cu_{22}$, $Pt_{54}Cu_{46}$ and $Pt_{37}Cu_{63}$ BANDs are 50.8, 50.78, 41.03, and 27.71 m^2/g_{Pt}. Among them, Pt NDs and $Pt_{78}Cu_{22}$ BANDs exhibited a high ECSA, around half (60%) of commercial Pt/C (84.76 m^2/g_{Pt}), owing to their highly branched structures and monodisperse properties.

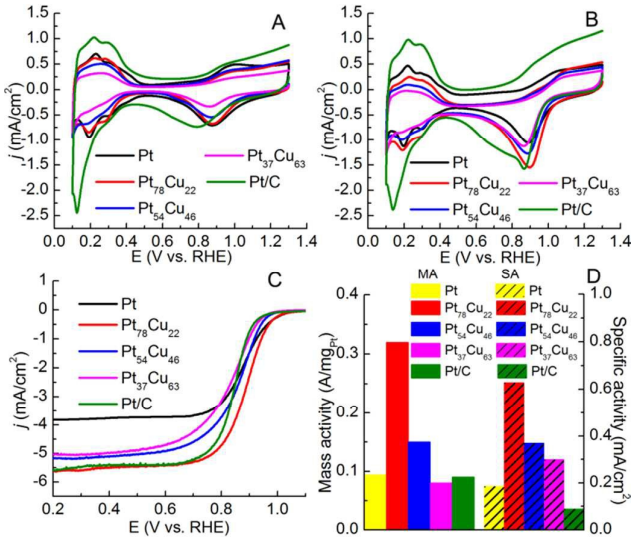

Figure 4. CV curves of as-prepared Pt NDs, PtCu BANDs and commercial Pt/C catalysts in N_2 (A) and O_2-saturated (B) 0.1 M $HClO_4$ solutions. (C) LSV curves of Pt NDs, PtCu BANDs and commercial Pt/C catalysts in O_2-saturated 0.1 M $HClO_4$ solutions with a scan rate of 20 mV/s. (D) Mass activity and specific activity of Pt NDs, PtCu BANDs and commercial Pt/C catalysts at 0.9 V.

In addition, a series of ORR measurements were also performed in O_2-saturated 0.1 M $HClO_4$ solution. The curves were all normalized by the geometrical area of the electrode (0.196 cm^2). Figure 4B shows the CV curves of Pt NDs, $Pt_{78}Cu_{22}$, $Pt_{54}Cu_{46}$ and $Pt_{37}Cu_{63}$ BANDs, as well as commercial Pt/C catalyst. All the catalysts present electrocatalytic abilities for ORR. Moreover, Pt NDs and PtCu BANDs exhibit a more positive onset and peak potential compared to commercial Pt/C catalyst. This shift might be caused by the high porosity as well as the decrease of desorption free energy of Pt-OH and Pt-O species due to the alloys formation between Pt and Cu.[28] Thus, the better catalytic activities for ORR could be expected as a result of the faster desorption rate. The ORR linear sweep voltammetry (LSV) curves of BANDs were obtained by using an RDE with a rotating rate of 1600 rpm, as shown in Figure 4C. The curves reveal two distinct potential regions: the diffusion controlled region bellow 0.6 V and the mixed kinetic-diffusion controlled region between 0.6 and 1.1 V. A more positive onset potential was observed on $Pt_{78}Cu_{22}$ BANDs (0.988 V) compared with commercial Pt/C catalyst (0.926 V). In addition, a positive shift of half-wave potential (42 mV) was also presented on $Pt_{78}Cu_{22}$ BANDs. In order to provide a further comparison on different catalysts, the kinetic currents, which were calculated from the LSV curves according to the Levich-Koutecky equation,[29] were normalized by Pt loading amount and ECSA, respectively. As illustrated in Figure 4D, the as-prepared PtCu BANDs exhibit larger mass activity (MA) and specific activity (SA) compared to commercial Pt/C catalyst at 0.9 V. For the PtCu BANDs, the MA was decreased with the increase of Cu content. Similar trend could also be observed for SA. In particular, the MA of $Pt_{78}Cu_{22}$ BANDs was 0.32 A/mg_{Pt}, which was much higher than that of commercial Pt/C catalyst (0.09 A/mg_{Pt}) as well as some reported works.[30,31] Additionally, the calculated SA of $Pt_{78}Cu_{22}$ BANDs (0.63 mA/cm^2) was more than 6 times greater than that of Pt/C (0.1 mA/cm^2).

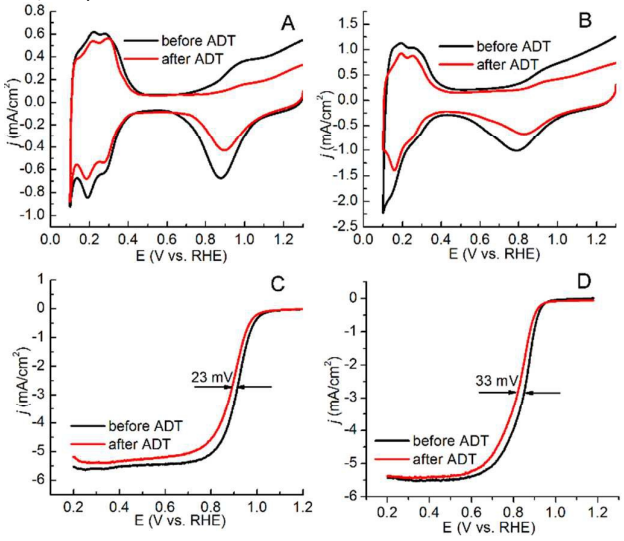

Figure 5. LSV curves of $Pt_{78}Cu_{22}$ BANDs (A) and commercial Pt/C catalysts (B) in N_2-saturated 0.1 M $HClO_4$ solution before and after ADT. CV curves of $Pt_{78}Cu_{22}$ BANDs (C) and commercial Pt/C catalysts (D) in O_2-saturated 0.1 M $HClO_4$ solutions at 1600 rpm before and after ADT.

The electrocatalytic durability of $Pt_{78}Cu_{22}$ BANDs and commercial Pt/C catalysts were evaluated using accelerated degradation test (ADT), which was performed by potential cycling between 0.6 to 1.1 V vs. RHE in O_2-saturated 0.1 M $HClO_4$ solution with a sweep rate of 100 mV/s. As illustrated in Figure 5, $Pt_{78}Cu_{22}$ BANDs showed 12% loss of ECSA, while there was 37% loss for commercial Pt/C after 5000 cycles. Furthermore, there were smaller changes (23 mV on half-wave potential) on LSA curves after ADT of $Pt_{78}Cu_{22}$ BANDs than that of Pt/C catalyst (33 mV on half-wave potential), indicating the better stability of $Pt_{78}Cu_{22}$ BANDs. The morphologies of $Pt_{78}Cu_{22}$ BANDs and commercial Pt/C catalysts after the stability test were also examined by TEM. Figure S3 reveals that the dendritic structures were maintained pretty well after ADT for $Pt_{78}Cu_{22}$ BANDs. In contrast, commercial Pt/C catalyst presented serious aggregation. The better stability of PtCu BANDs should be attributed to the introduction of highly

branched PtCu BANDs, which could significantly mitigate the Ostwald ripening and aggregation of Pt as well as corrosion of the carbon support.[32-35]

Several specific features of PtCu BANDs should contribute to the enhanced electrocatalytic activity and durability: (1) the porous PtCu BANDs possess high surface areas due to the unique open structure. Moreover, the branches could provide many active sites, which are favorable for ORR.[5, 36] (2) The geometric effects in PtCu BANDs also play an important role on the improvement of electrocatalytic activities. It has been proved that the existence of certain strains in PtCu bimetallic alloy could boost the overall activity.[12] The compressive lattice strain in Pt lattice, induced by the insert of Cu, could lead to the downshift of the d-band center. This downshift was demonstrated to decrease the adsorption energy between Pt and O, which is beneficial to ORR.[12, 37] (3) The superior stability of PtCu BANDs over carbon-supported Pt materials should be ascribed to the elimination of carbon corrosion which is the main degradation pathway in traditional catalysts.[13] Moreover, the highly branched nanodendritic structures make the materials less vulnerable to Ostwald ripening as well as aggregation, and thus the durability was increased.[35]

Conclusions

In summary, we have developed a very simple and efficient wet-chemical strategy for high-yield (~100%) synthesis of PtCu BANDs. The ratio between Pt and Cu played an important role on the dendritic structure of the final product. The MA of as-prepared $Pt_{78}Cu_{22}$ BANDs was nearly 4 times greater than that of commercial Pt/C catalyst. In terms of SA, the $Pt_{78}Cu_{22}$ BANDs were 6-fold more active than Pt/C catalyst. The high electrocatalytic activity and stability for ORR should be attributed to the unique dendritic structure, high surface, as well as the elimination of carbon support. Therefore, this synthesis approach might provide a new platform for further engineering morphology and composition, which could significantly impact broad areas including fuel cells, batteries, and so on.

Acknowledgement

This work was supported by a startup fund of Washington State University, USA. We thank Franceschi Microscopy & Image Center at Washington State University for TEM measurements. We also thank Jing Li in Shandong University for the HAADF-STEM and EDS elemental mapping.

Note and References

* chengzhou.zhu@wsu.edu, yuehe.lin@wsu.edu

1 C. Z. Zhu, H. Li, S. F. Fu, D. Du, Y. H. Lin, *Chem. Soc. Rev.*, 2016, DOI: 10.1039/C5CS00670H.
2 W. T. Yu, M. D. Porosoff and J. G. G. Chen, *Chem. Rev.*, 2012, **112**, 5780-5817.
3 C. Baldizzone, S. Mezzavilla, H. W. P. Carvalho, J. C. Meier, A. K. Schuppert, M. Heggen, C. Galeano, J. D. Grunwaldt, F. Schuth and K. J. J. Mayrhofer, *Angew. Chem. Int. Edit.*, 2014, **53**, 14250-14254.
4 C. Chen, Y. J. Kang, Z. Y. Huo, Z. W. Zhu, W. Y. Huang, H. L. L. Xin, J. D. Snyder, D. G. Li, J. A. Herron, M. Mavrikakis, M. F. Chi, K. L. More, Y. D. Li, N. M. Markovic, G. A. Somorjai, P. D. Yang and V. R. Stamenkovic, *Science*, 2014, **343**, 1339-1343.
5 X. Q. Huang, E. B. Zhu, Y. Chen, Y. J. Li, C. Y. Chiu, Y. X. Xu, Z. Y. Lin, X. F. Duan and Y. Huang, *Adv. Mater.*, 2013, **25**, 2974-2979.
6 C. Z. Zhu and S. J. Dong, *Nanoscale*, 2013, **5**, 1753-1767.
7 S. J. Guo, S. Zhang and S. H. Sun, *Angew. Chem. Int. Edit.*, 2013, **52**, 8526-8544.
8 L. Han, H. Liu, P. L. Cui, Z. J. Peng, S. J. Zhang and J. Yang, *Sci. Rep.*, 2014, **4**, 1-8.
9 S. J. Guo and S. H. Sun, *J. Am. Chem. Soc.*, 2012, **134**, 2492-2495.
10 A. Oh, H. Baik, D. S. Choi, J. Y. Cheon, B. Kim, H. Kim, S. J. Kwon, S. H. Joo, Y. Jung and K. Lee, *ACS Nano*, 2015, **9**, 2856-2867.
11 D. L. Wang, H. L. L. Xin, R. Hovden, H. S. Wang, Y. C. Yu, D. A. Muller, F. J. DiSalvo and H. D. Abruna, *Nat. Mater.*, 2013, **12**, 81-87.
12 P. Strasser, S. Koh, T. Anniyev, J. Greeley, K. More, C. F. Yu, Z. C. Liu, S. Kaya, D. Nordlund, H. Ogasawara, M. F. Toney and A. Nilsson, *Nat. Chem.*, 2010, **2**, 454-460.
13 J. A. Wittkopf, J. Zheng and Y. S. Yan, *ACS Catal.*, 2014, **4**, 3145-3151.
14 L. Ma, C. M. Wang, B. Y. Xia, K. K. Mao, J. W. He, X. J. Wu, Y. J. Xiong and X. W. Lou, *Angew. Chem. Int. Edit.*, 2015, **54**, 5666-5671.
15 L. Wang, Y. Nemoto and Y. Yamauchi, *J. Am. Chem. Soc.*, 2011, **133**, 9674-9677.
16 L. Wang, M. Imura and Y. Yamauchi, *ACS Appl. Mater. Inter.*, 2012, **4**, 2865-2869.
17 C. Z. Zhu, D. Du, A. Eychmüller, Y. H. Lin, *Chem. Rev.*, 2015, **115**, 8896-8943.
18 L. Wang, H. J. Wang, Y. Nemoto and Y. Yamauchi, *Chem. Mater.*, 2010, **22**, 2835-2841.
19 Z. Cai, Y. Kuang, X. H. Qi, P. Wang, Y. Zhang, Z. C. Zhang and X. M. Sun, *J. Mater. Chem. A*, 2015, **3**, 1182-1187.
20 Y. M. Tan, J. M. Fan, G. X. Chen, N. F. Zheng and Q. J. Xie, *Chem. Commun.*, 2011, **47**, 11624-11626.
21 V. Tzitzios, D. Niarchos, M. Gjoka, N. Boukos and D. Petridis, *J. Am. Chem. Soc.*, 2005, **127**, 13756-13757.
22 Y. J. Song, Y. Yang, C. J. Medforth, E. Pereira, A. K. Singh, H. F. Xu, Y. B. Jiang, C. J. Brinker, F. van Swol and J. A. Shelnutt, *J. Am. Chem. Soc.*, 2004, **126**, 635-645.
23 H. J. Wang, L. Wang, T. Sato, Y. Sakamoto, S. Tominaka, K. Miyasaka, N. Miyamoto, Y. Nemoto, O, Terasaki, and Y. Yamauchi, *Chem. Mater.*, 2012, **24**, 1591-1598.
24 P. A. Ganesh and D. Jeyakumar, *Nanoscale*, 2014, **6**, 13012-13021.
25 S. Tominaka, M. Shigeto, H. Nishizeko, and T. Osaka, *Chem. Commun.*, 2010, **46**, 8989-8991.
26 H. Zhu, M. L. Du, D. L. Yu, Y. Wang, L. N. Wang, M. L. Zou, M. Zhang and Y. Q. Fu, *J. Mater. Chem. A*, 2013, **1**, 919-929.
27 C. G. Arellano, R. Luque and D. J. Macquarrie, *Chem. Commun.*, 2009, **30**, 4581-4583.
28 K. Zhang, Q. L. Yue, G. F. Chen, Y. L. Zhai, L. Wang, H. S. Wang, J. S. Zhao, J. F. Liu, J. B. Jia and H. B. Li, *J. Phys. Chem. C*, 2011, **115**, 379-389.
29 H. Zhang, M. S. Jin, J. G. Wang, W. Y. Li, P. H. C. Camargo, M. J. Kim, D. R. Yang, Z. X. Xie and Y. A. Xia, *J. Am. Chem. Soc.*, 2011, **133**, 6078-6089.
30 M. Wang, W. M. Zhang, J. Z. Wang, A. Minett, V. Lo, H. K. Liu, and J. Chen, *J. Mater. Chem. A*, 2013, **7**, 2391-2394.

31 Y. C. Tseng, H. S. Chen, C. W. Liu, T. H. Yeh, and K. W. Wang, *J. Mater. Chem. A*, 2014, **12**, 4270-4275.
32 K. Hartl, M. Nesselberger, K. J. J. Mayrhofer, S. Kunz, F. F. Schweinberger, G. Kwon, M. Hanzlik, U. Heiz and M. Arenz, *Electrochim. Acta.*, 2010, **56**, 810-816.
33 F. J. Perez-Alonso, C. F. Elkjaer, S. S. Shim, B. L. Abrams, I. E. L. Stephens and I. Chorkendorff, *J. Power Sources*, 2011, **196**, 6085-6091.
34 Y. Shao-Horn, W. C. Sheng, S. Chen, P. J. Ferreira, E. F. Holby and D. Morgan, *Top. Catal.*, 2007, **46**, 285-305.
35 S. H. Sun, G. X. Zhang, D. S. Geng, Y. G. Chen, R. Y. Li, M. Cai and X. L. Sun, *Angew. Chem. Int. Edit.*, 2011, **50**, 422-426.
36 B. Lim, M. J. Jiang, P. H. C. Camargo, E. C. Cho, J. Tao, X. M. Lu, Y. M. Zhu and Y. N. Xia, *Science*, 2009, **324**, 1302-1305.
37 M. Mavrikakis, B. Hammer and J. K. Norskov, *Phys. Rev. Lett.*, 1998, **81**, 2819-2822.

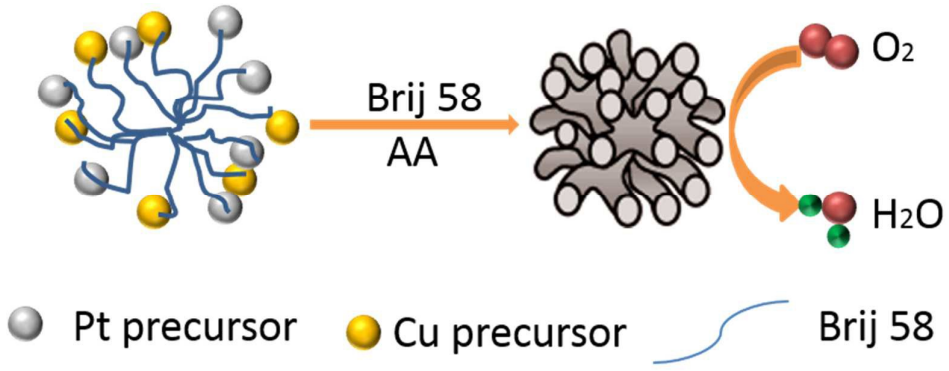

The highly branched PtCu bimetallic alloy nanodendrites were synthesized by a facile chemical reduction method using Brij 58 as the soft template. The as-prepared alloys presented superior electrocatalytic activities for oxygen reduction reaction.